Quercetin protects against atherosclerosis by regulating the expression of PCSK9, CD36, PPARγ, LXRα and ABCA1

QINGLING JIA*, HUI CAO*, DINGZHU SHEN, SHANSHAN LI, LI YAN, CHUAN CHEN, SANLI XING and FANGFANG DOU

Shanghai Geriatric Institute of Chinese Medicine, Shanghai University of Traditional Chinese Medicine, Shanghai 200031, P.R. China

Received January 7, 2019; Accepted July 1, 2019

DOI: 10.3892/ijmm.2019.4263

Abstract. The aim of this study was to investigate the mechanisms through which quercetin protects against atherosclerosis (AS) in apoE$^{-/-}$ mice by regulating the expression of proprotein convertase subtilisin/kexin type 9 (PCSK9), cluster of differentiation 36 (CD36), peroxisome proliferator-activated receptor γ (PPARγ), liver X receptor α (LXRα) and ATP binding cassette transporter A1 (ABCA1). We established an animal model of high-fat diet induced AS using apoE$^{-/-}$ mice. H&E, Oil Red O and Masson's trichrome staining were performed on aortic sinus and liver tissue sections to evaluate the histopathology, lipid accumulation and collagen deposition, respectively. Filipin staining was performed to detect free cholesterol (FC) in the aortic sinus. ELISA was performed to measure the serum levels of lipids including total cholesterol (TC), triglyceride (TG), high-density lipoprotein-cholesterol (HDL-C), low-density lipoprotein-cholesterol (LDL-C) and oxidized low-density lipoprotein (oxLDL), as well as the levels of inflammatory cytokines, including tumor necrosis factor (TNF)-α, interleukin (IL)-6 and IL-10. Western blot analysis was performed to analyze the protein expression levels of PCSK9, CD36, PPARγ, LXRα and ABCA1 in both the aorta and liver tissue. H&E staining revealed the presence of atherosclerotic plaques in the aortic sinus. Oil Red O staining revealed the existence of massive red-stained lipids in the aortic sinus and Masson's trichrome staining revealed decreased collagen fibers and increased plaque instability. Filipin staining revealed that free cholesterol levels in the aorta sinus were increased. In addition, H&E staining suggested hepatocyte structural disorder in the model group, and Oil Red O staining revealed a cytoplasm filled with lipid droplets, which contained a large amount of red-stained lipids. Masson's trichrome staining revealed that the liver tissue of the model group had fewer collagen fibers compared with that of the control group. Moreover, the mice in the model group had higher serum TC, LDL-C, oxLDL, TNF-α and IL-6 levels, and lower IL-10 levels. The protein expression levels of PCSK9 and CD36 were increased, while those of PPARγ, LXRα and ABCA1 were decreased in the aortas and livers of the model group mice. However, treatment with quercetin attenuated all these effects. On the whole, these results demonstrate that quercetin prevents the development of AS in apoE$^{-/-}$ mice by regulating the expression of PCSK9, CD36, PPARγ, LXRα and ABCA1.

Correspondence to: Dr Dingzhu Shen, Shanghai Geriatric Institute of Chinese Medicine, Shanghai University of Traditional Chinese Medicine, 365C Xiangyang South Road, Xuhui, Shanghai 200031, P.R. China
E-mail: 13818279131@163.com

*Contributed equally

Key words: quercetin, atherosclerosis, proprotein convertase subtilisin/kexin type 9, cluster of differentiation 36, peroxisome proliferator-activated receptor γ, liver X receptor α, ATP binding cassette transporter A1

Introduction

Atherosclerosis (AS) is a complex disease involving a number of factors, of which, lipid metabolism disorders are key mediators. Reverse cholesterol transport (RCT) is a process that occurs when free cholesterol (FC) is transferred to high-density lipoprotein (HDL), moves to the liver, and is excreted as bile acid (1). Proprotein convertase subtilisin/kexin type 9 (PCSK9) plays a direct role in the RCT pathway and may influence relevant steps in the pathogenesis and development of AS (2). Cluster of differentiation 36 (CD36) affects the RCT process and consequently affects the pathogenesis and development of AS by regulating the expression of liver X receptors (LXRs) (3). Elevated levels of PCSK9 stimulate the expression of CD36 and the uptake of oxidized low-density lipoprotein (oxLDL) in tumor necrosis factor (TNF)-α-treated macrophages, thus contributing to the progression of AS (4). The peroxisome proliferator-activated receptor γ (PPARγ)/LXRα/ATP binding cassette transporter A1 (ABCA1) pathway can be activated to influence the efflux of cholesterol from macrophages, and thus plays important roles in the pathogenesis of AS (5).

Quercetin is a flavonoid that has been shown to exert cardiovascular protective effects and anti-atherosclerotic effects (6). Quercetin can be used to effectively treat AS by regulating the expression of PCSK9 and ABCA1 in RAW264.7

macrophages (7). Quercetin exerts anti-atherogenic effects by promoting the efflux of cholesterol from macrophages by upregulating the gene expression of PPARγ, LXRα and ABCA1 (8). In this study, apoE$^{-/-}$ mice fed with a high-fat diet and male C57BL/6 mice of the same age were used as the study animals. The Chinese medicine monomer, quercetin, was used as an intervention, and the western medicine, atorvastatin, was used as a positive control. The general condition and body-weight dynamics of the mice were observed. H&E, Oil Red O and Masson's trichrome staining were used to detect the pathological morphology, lipid accumulation and collagen deposition in the aortic sinus and liver tissues of mice, and the serum lipids in the peripheral blood of mice were measured by ELISA. The expression levels of PCSK9, CD36, PPARγ, LXRα and ABCA1 in the mouse aortas and liver tissues were measured by western blot analysis. Based on the results of these analyses, a deeper insight into the preventive effects of quercetin against AS was gained.

Materials and methods

Experimental animals. Specific pathogen-free (SPF) 12-week-old male apoE$^{-/-}$ mice [license no. SCKX (Jing) 2016-0011] and male C57BL/6 mice at an identical age and strain [license no. SCKX (Jing) 2016-0006] were purchased from Beijing Vital River Laboratory Animal Technology Co., Ltd. The Animals were single-housed, and the cages were kept in an SPF environment with a controlled temperature of 24±1˚C, a humidity of 50-70%, and a light/dark cycle of 12/12 h. All animal experiments were approved and carried out in strict compliance with the Shanghai University of Traditional Chinese Medicine Institutional Animal Care and Use Committee (IACUC) guidelines (Protocol no. PZSHUTCM18113002).

Medicine and major reagents. Quercetin (B20527) was supplied by Shanghai YuanYe Biotechnology Co., Ltd. Atorvastatin (H20051408) was obtained from Pfizer Inc. Mouse low-density lipoprotein-cholesterol (LDL-C), high-density lipoprotein-cholesterol (HDL-C), triglyceride (TG), total cholesterol (TC), TNF-α, interleukin (IL)-6 and IL-10 ELISA kits (EK-M21272, EK-M21273, EK-M21274, EK-M21275, EK-M21159, EK-M20193 and EK-M20153) were obtained from EK-Bioscience. The mouse oxLDL ELISA kit (H-20710) was obtained from Shanghai Hengyuan Biotechnology Co., Ltd. Rabbit anti-PCSK9 (ab95478), rabbit anti-CD36 (ab133625), rabbit anti-PPARγ (ab59256) and mouse anti-LXRα (ab41902) antibodies were obtained from Abcam. Mouse anti-ABCA1 (MA5-16026) antibody was obtained from Thermo Fisher Scientific. Rabbit anti-GAPDH (#5174S), HRP-linked anti-rabbit IgG (#7074P2) and HRP-linked anti-mouse IgG (#7076P2) were obtained from Cell Signaling Technology. RIPA lysis buffer (P0013B), PMSF (ST505), the BCA protein assay kit (P0010), SDS-PAGE protein loading buffer (5X) (P0015L), SDS-PAGE gel preparation kit (P0012A), Protein ladder (P0071) and BeyoECL Plus (P0018S) were obtained from Shanghai Beyotime Biotechnology Co., Ltd. EZ-Buffers H 10X TBST buffer (C520009) was supplied by Shanghai Sangon Biotechnology Co., Ltd. Mayer hematoxylin staining reagent (1092490500) was supplied by Merck KGaA. Erythrosine (053-00252) was obtained from Wako pure chemical industries, Ltd. Oil Red O staining (G1016) was supplied by Servicebio technology Co., Ltd. Bright green SF light yellow (71022480) was supplied by Sinopharm Chemical Reagent Co., Ltd. The Filipin Staining kit (GMS80059.3) was obtained from Shanghai Genmed Gene Medicine Technology Co., Ltd.

Modeling and grouping. A total of 54 12-week-old apoE$^{-/-}$ mice were divided into 3 groups using a random number table method (9) after being fed a regular diet for 1 week. The 3 groups included apoE$^{-/-}$ mice fed with a high-fat diet (model group, n=18), apoE$^{-/-}$ mice fed with a high-fat diet and treated with quercetin (quercetin group, n=18) and apoE$^{-/-}$ mice fed with a high-fat diet and treated with atorvastatin (atorvastatin group, n=18). The high-fat diet included 21% fat and 0.5% cholesterol, but otherwise was a normal diet. The C57BL/6 mice, at an identical age and strain, were fed with a normal diet and served as the control group (control group, n=18). The quercetin group and atorvastatin group received via oral gavage (once per day for 12 weeks), quercetin water solution (12.5 mg/kg) and atorvastatin water solution (2.06 mg/kg), respectively. The doses of quercetin and atorvastatin were calculated using a human equivalent dose formula based on 60 kg adults. The control group and model group received via oral gavage, equal volumes of distilled water (once per day for 12 weeks).

General morphological observation of the mice. The general condition of the animals' health, including body type, coat color, behavior, food consumption and body weight were observed and recorded weekly.

Histopathological examination, lipid accumulation and collagen deposition evaluation in mouse aortas and livers. The mice were anesthetized with 0.05 ml, 2% sodium pentobarbital via intraperitoneal (IP) injection (anesthesia dose of 50 mg/kg) (9). Perfusion fixation was then performed using 4% paraformaldehyde. The segment of the aorta ranging from the arch to the abdominal aorta and the liver were harvested and fixed in 10% formaldehyde for the paraffin-embedded or frozen sectioning (-15˚C). The tissue sections were subjected to hematoxylin and eosin (H&E) staining, Masson's trichrome staining and Oil Red O staining (room temperature). The histopathological examination of the aorta and liver was performed under an Olympus BH2 microscope. H&E, Masson's trichrome and Filipin staining results of the aortic sinus were observed and photographed using a Nikon 4500 digital camera (Nikon). Oil Red O, H&E and Masson's trichrome staining results of the liver were scanned using a Pannoramic MIDI digital scanner (3D Histech). Subsequently, semi-quantification was performed using the following formula: Area of plaque (PA, mm^2) = vessel area (IE, mm^2)-lumen area (LA, mm^2), adjusted PA = PA/IE-LA. The collagen fiber content = the area of Masson's trichrome-stained collagen/lumen area. The lipid content = the Oil Red O stained area/lumen area.

Detection of aortic FC using Filipin staining. A FC Filipin fluorescent staining kit (frozen section-based) was purchased from Shanghai Genmed Gene Medicine Technology Co., Ltd.

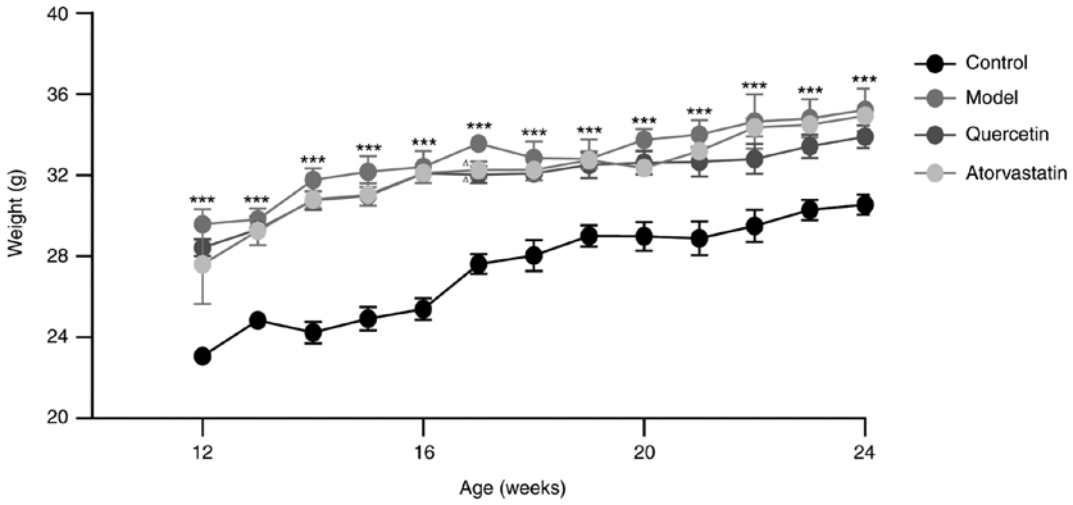

Figure 1. The dynamic body weights of the mice. ***P<0.001, compared with the control group; ΔP<0.05, compared with the model group.

and used to detect the FC levels in the aortic sinus according to the manufacturer's instructions. The slides were covered with a coverslip immediately after staining (room temperature) and then observed under a fluorescence microscope (Olympus BX51, Olympus) immediately. The excitation wavelength and emission wavelength were 340 and 430 nm, respectively. The cholesterol deposits exhibited blue fluorescence after staining.

Determination of mouse serum levels of TC, TG, LDL-C, HDL-C and oxLDL using ELISA. The animals were fasted and then anesthetized with 2% sodium pentobarbital. Blood was then collected from the retro-orbital sinus after eyeball removal, followed by euthanasia. The blood was allowed to settle for 2 h, and was then centrifuged at 4˚C, 13,523 x g, for 30 min. The supernatant was harvested and used for ELISA according to the instructions provide with the kit manuals. The serum levels of TC, TG, LDL-C, HDL-C and oxLDL were determined at OD 450 nm and corresponded to standard curves.

Determination of mouse serum levels of TNF-α, IL-6 and IL-10 using ELISA. Mouse serum was prepared as described above. ELISA was performed according to the instructions provided with the kit manual. The serum levels of TNF-α, IL-6 and IL-10 were determined at OD 450 nm and corresponded to standard curves.

Western blot analysis of protein expression levels of PCSK9, CD36, PPARγ, LXRα and ABCA1 in mouse aorta and liver samples. Proteins were extracted from aorta and liver tissues with RIPA lysis buffer containing PMSF. This was followed by centrifugation at 13,523 x g at 4˚C for 30 min, and the supernatant was then collected for protein quantification using the BCA method. Samples were mixed with 5X loading buffer and heated in boiling water for 10 min to denature the proteins. These treated samples were separated on a 12% SDS-PAGE gel (70 V, 30 min, and then 120 V, 90 min), the proteins were transferred to PVDF membranes following a wet transfer protocol (270 mA, 90 min). The membranes were then blocked in 5% non-fat milk solution for 2 h at room temperature, and then incubated with primary antibodies against PCSK9 (1:1,000), CD36 (1:1,000), PPARγ (1:1,000), LXRα (1:1,000), ABCA1 (1:1,000) and GAPDH (1:3,000) overnight at 4˚C. The membranes were then washed by TBST buffer for 10 min 3 times and then incubated with HRP-labeled secondary antibodies (1:1,000) for 1 h at room temperature. After washing 10 min 3 times, the membranes were incubated with a 1:1 mixture of solution BeyoECL Plus A and BeyoECL Plus B according to the manual of the ECL kit. The PVDF membranes were then visualized using an Invitrogen iBright Imaging System (FL1000, Thermo Fisher Scientific). The integrated absorbance (IA = mean grey value x area) of the protein bands was measured using Image J software. The target protein expression level was presented as the ratio of the IA of the target protein to the IA of GAPDH.

Statistical analysis. The data were analyzed using SPSS21.0 software. The numerical data are presented as the means ± standard deviation ($\bar{x}$ ± s). The categorical data from repeated measurements were analyzed by variance analysis. Comparisons among multiple randomized groups were performed using one-way ANOVA, followed by Student-Newman-Keuls (SNK) comparison between any 2 groups. The significance level α was set at 0.05 (two-sided) and a P-value of 0.05 was considered to indicate a statistically significant difference. The data were plotted using GraphPad Prism 5 Project software.

Results

General health conditions. The mice in the control group were in a good condition, with shiny coats and agile movements. The mice in the model group had become overweight, had coats with dry hair and slow movements. Compared with the mice in the model group, the mice in both the quercetin and atorvastatin groups were in a relatively better condition, with shinier coats and more agile movements. The mice in all the groups exhibited normal food consumption during the experimental period.

Table I. Comparison of serum lipid levels in each group.

Group	n	TC	TG	LDL-C	HDL-C	oxLDL
A	6	6.22±0.64	5.36±0.48	2.42±0.37	5.16±0.29	180.04±3.33
B	6	7.91±0.85[a]	5.77±0.32	3.15±0.46[a]	4.05±0.60[a]	242.46±3.93[b]
C	6	6.83±0.87[c]	6.13±0.45	2.48±0.41[d]	4.39±0.40	204.11±2.67[e]
D	6	6.46±0.83[d]	6.00±0.17	2.47±0.34[d]	4.41±0.78	199.24±4.29[e]

Data are presented as the means ± standard deviation. A, control group; B, model group; C, quercetin group; D, atorvastatin group. As compared with the control group: [a]P<0.01, [b]P<0.001; as compared with the model group: [c]P<0.05, [d]P<0.01 and [e]P<0.001. TC, total cholesterol; TG triglyceride; LDL-C, low-density lipoprotein-cholesterol; HDL-C, high-density lipoprotein-cholesterol. The levels of TC, TG, LDL-C and HDL-C are shown in nmol/l; oxLDL levels are shown in μg/l.

Table II. Comparison of serum TNF-α, IL-6 and IL-10 levels in each group of mice.

Group	n	TNF-α	IL-6	IL-10
A	6	433.14±52.46	65.73±4.59	311.94±20.96
B	6	510.12±50.28[a]	77.14±7.06[a]	252.12±37.28[a]
C	6	437.78±19.61[b]	67.45±5.28[b]	305.81±35.90[b]
D	6	436.05±38.25[b]	66.27±4.85[b]	307.10±26.37[b]

Data are presented as the means ± standard deviation and are shown in nmol/l. A, control group; B, model group; C, quercetin group; D, atorvastatin group. As compared with the control group: [a]P<0.01; as compared with the model group: [b]P<0.01. TNF-α, tumor necrosis factor-α; IL, interleukin.

One-way ANOVA of repeated measurements revealed that there was no interaction between the groups and intervention time (P>0.05). The main effect caused by grouping and intervention time was statistically significant (P<0.05). The body weight of the model mice differed significantly from that of the control mice (P<0.05). Compared with the model group, significant differences were also observed in the quercetin and atorvastatin groups (P<0.05); however, the differences between the quercetin and the atorvastatin group were not significant (P>0.05). One-way ANOVA analysis revealed that the model group differed significantly at each time point (12-24 weeks) compared with the control group (P<0.001). The quercetin and the atorvastatin group exhibited significant differences compared to the model group (P<0.05) at week 17. The detailed data are presented in Fig. 1.

Serum lipid profile. In the model group, the serum levels of TC, LDL-C and oxLDL increased significantly (P<0.01 and P<0.001), while those of HDL-C decreased significantly (P<0.01), as compared with the control group. The mice in the quercetin and atorvastatin groups exhibited significantly lower serum levels of TC, LDL-C and oxLDL than the mice in the model group (P<0.05, P<0.01, P<0.001). However, the differences between the quercetin and atorvastatin group were not significant (P>0.05). The detailed results are presented in Table I.

Serum levels of TNF-α, IL-6 and IL-10. In the model group, the serum levels of TNF-α and IL-6 increased significantly (P<0.01), while those of IL-10 decreased significantly compared with the control group (P<0.01). Compared with the model group, the quercetin and atorvastatin groups exhibited lower levels of TNF-α and IL-6 (P<0.01) and higher levels of IL-10 (P<0.01). However, the differences between the quercetin and atorvastatin group were not significant (P>0.05). The detailed results are presented in Table II.

Pathological examination of mouse aortic tissue

H&E staining. In the model group, a greater amount of atherosclerotic plaque was observed at the aortic root than the control group (P<0.001). Compared with the model group, the areas of atherosclerotic plaque in both the quercetin and atorvastatin groups were much smaller (P<0.01). However, the area of atherosclerotic plaque did not differ significantly between the quercetin and atorvastatin group (P>0.05). The detailed data are presented in Fig. 2.

Oil Red O staining. In the model group, atherosclerotic plaque development was observed at the aortic root area, with the intimal thickening of the aorta, and an increased amount of massive Oil Red O-stained lipids (P<0.001), as compared with the control group. The amount of Oil Red O-stained lipids in the quercetin and atorvastatin groups decreased significantly compared with the model group (P<0.05). However, the difference between the quercetin and atorvastatin group was not significant (P>0.05). The detailed data are presented in Fig. 3.

Masson's trichrome staining. In the model group, the atherosclerotic plaques had thinner fibrous caps, with decreased

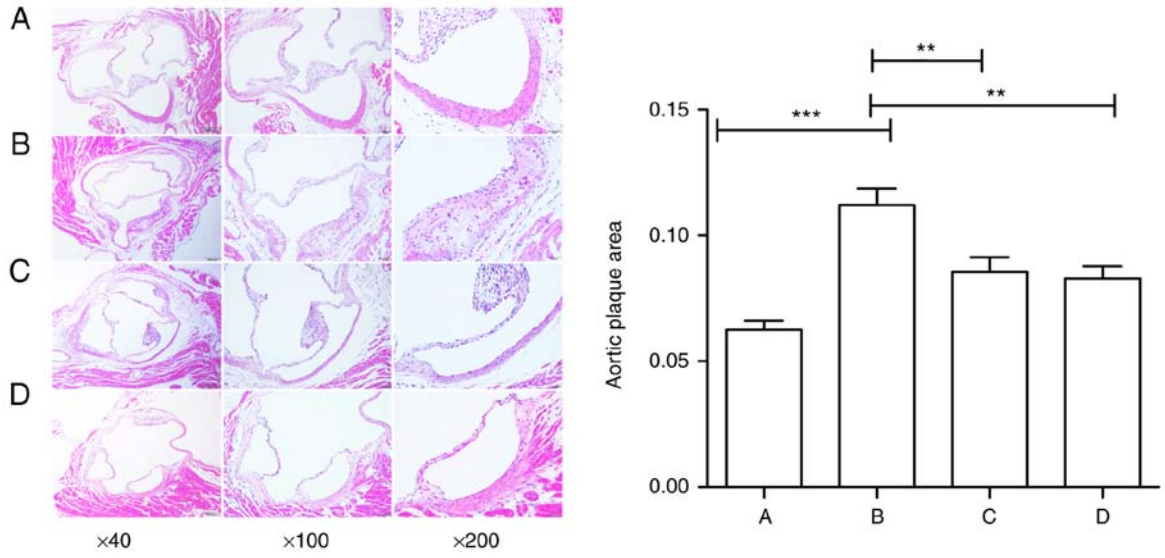

Figure 2. Effect of quercetin on aortic plaque area in mouse (H&E staining, x40, x100 and x200 magnification). (A) Control group; (B) model group; (C) quercetin group; (D) atorvastatin group. Scale bars, 100, 50 and 50 μm. Data are presented as the means ± standard deviation, **P<0.01 and ***P<0.001.

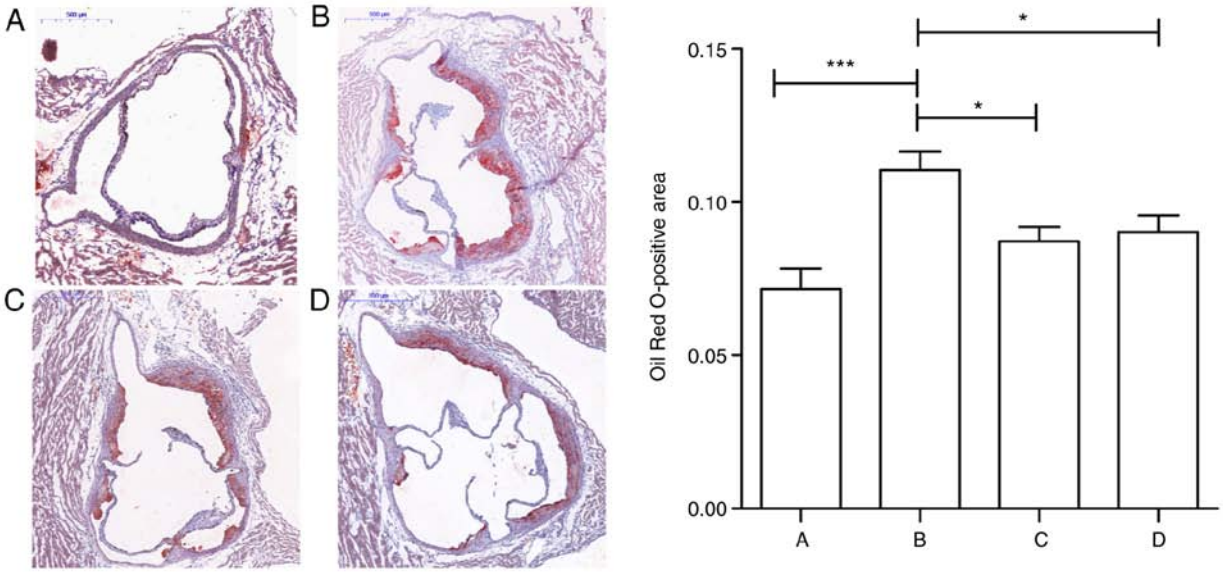

Figure 3. Effect of quercetin on the lipid area of mouse aorta red staining (Oil Red O staining, x40 magnification). (A) Control group; (B) model group; (C) quercetin group; (D) atorvastatin group. Scale bar, 500 μm. Data are presented as the means ± standard deviation, *P<0.05 and ***P<0.001.

collagen fibers and increased plaque instability, as assessed by Masson's trichrome staining (P<0.05), as compared with the control group. In the quercetin and atorvastatin groups, the collagen fiber content in the atherosclerotic plaques increased homogenously compared with the model group (P<0.05 and P<0.001). However, the difference between the quercetin and atorvastatin group was not statistically significant (P>0.05). The detailed data are presented in Fig. 4.

Filipin staining of mouse aorta sinus. The mice in the control group exhibited small amounts of FC in the aortic sinus, as assessed by Filipin staining. By contrast, the mice in the model group had more FC. The mice in the quercetin and the atorvastatin groups had lower amounts of FC in their aortic sinus atherosclerotic plaques. The results are shown in Fig. 5.

Pathological examination of mouse liver tissue. H&E staining revealed that the mice in the control group had a normal hepatic ultrastructure and no steatosis. The hepatocytes had an abundant cytoplasm and were centrally located around the nuclei. The cords of the hepatocytes were arranged radially around the central vein. By contrast, the mice in the model group had disorganized cords, deformed and compressed hepatocytes, and cytoplasmic accumulation of lipid droplets with varied size, number and shape. In the quercetin and atorvastatin groups, liver damage was less severe than the model group. Most of the hepatocytes had a normal ultrastructure, intact cell membranes and less lipid droplet accumulation.

Oil Red O staining revealed that the red-stained lipid droplets were distributed sparsely throughout hepatic tissue in the control group. By contrast, the mice in the model group

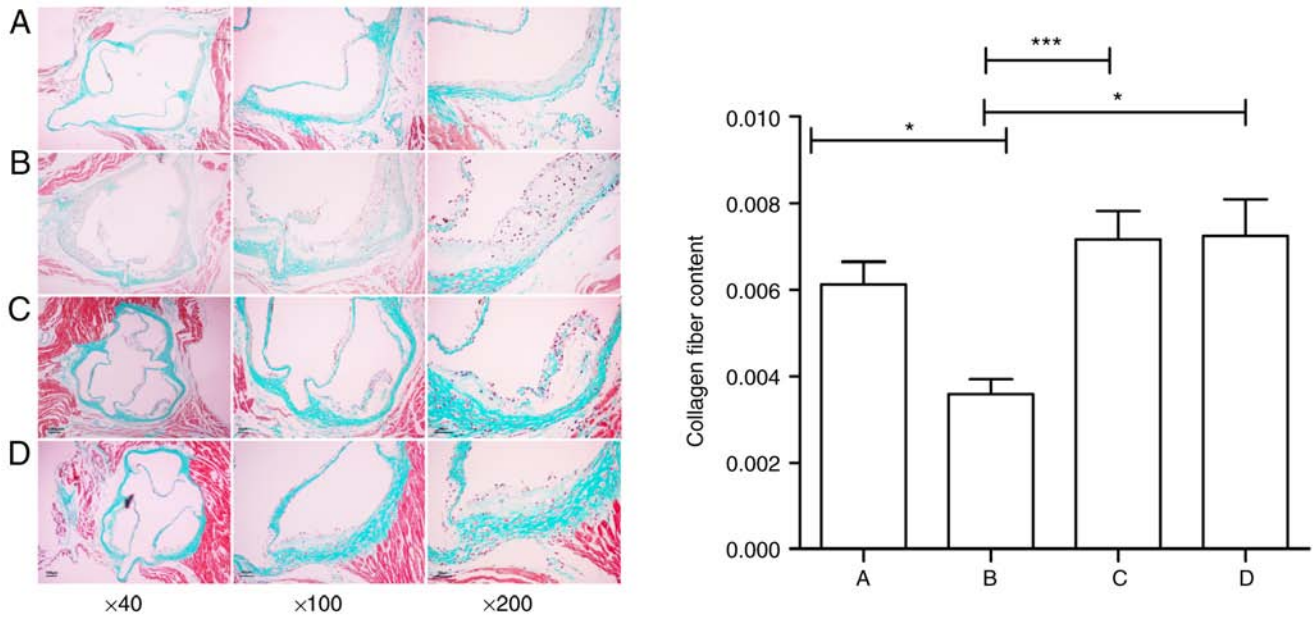

Figure 4. Effect of quercetin on the area of plaque collagen in mouse (Masson's trichrome staining, x40, x100 and x200 magnification). (A) Control group; (B) model group; (C) quercetin group; (D) atorvastatin group. Scale bars, 100, 50 and 50 μm. Data are presented as the means ± standard deviation, *P<0.05 and ***P<0.001.

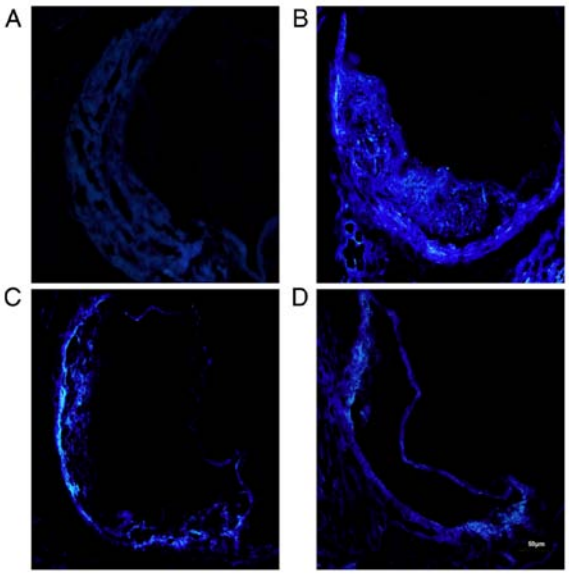

Figure 5. Free cholesterol accumulation in mouse aorta (Filipin staining, x200 magnification). (A) Control group; (B) model group; (C) quercetin group; (D) atorvastatin group.

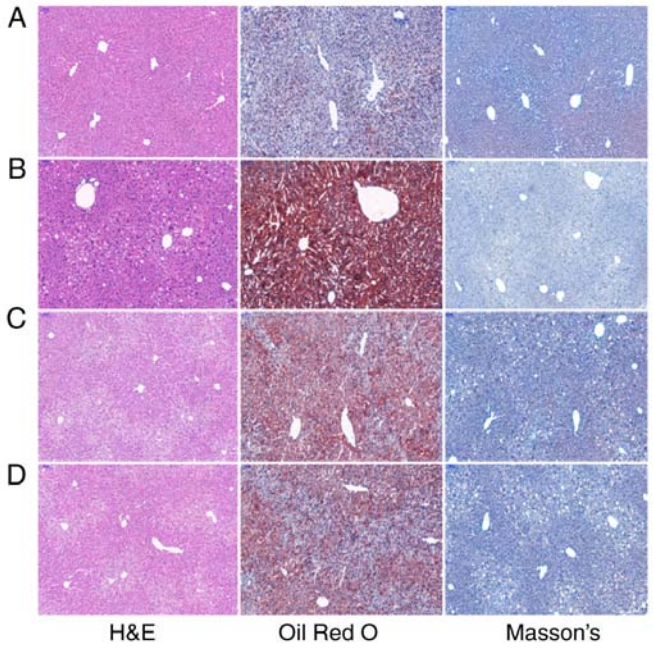

Figure 6. Histopathological examination, lipid accumulation and collagen deposition in mouse liver (H&E staining, Oil Red O staining and Masson's trichrome staining, x100 magnification). (A) Control group; (B) model group; (C) quercetin group; (D) atorvastatin group.

had a higher number of red-stained lipid droplets which accumulated in the hepatocytes. The number of hepatocytes with red-stained lipid droplets in the quercetin and atorvastatin groups decreased.

Masson's trichrome staining revealed that the mice in the control group had an amount of collagen fibers in their liver tissue. By contrast, the mice in the model group had thinner fibrous caps and less collagen fibers in their livers. Compared with the model group, the mice in the quercetin and atorvastatin group had homogeneously increased amounts of collagen fibers throughout the liver tissue. The results are presented in Fig. 6.

Protein expression levels of PCSK9, CD36, PPARγ, LXRα and ABCA1 in aortas and livers of mice. In the control group, the protein expression levels of PPARγ, LXRα and ABCA1 were high, while those of PCSK9 and CD36 were low in both the aorta and the liver. In the model group, the protein expression levels of PPARγ, LXRα and ABCA1 decreased (P<0.5 and P<0.01), while those of PCSK9 and CD36 increased (P<0.05 and P<0.001) in both the aorta and the liver as compared with the control group. Quercetin and atorvastatin treatment

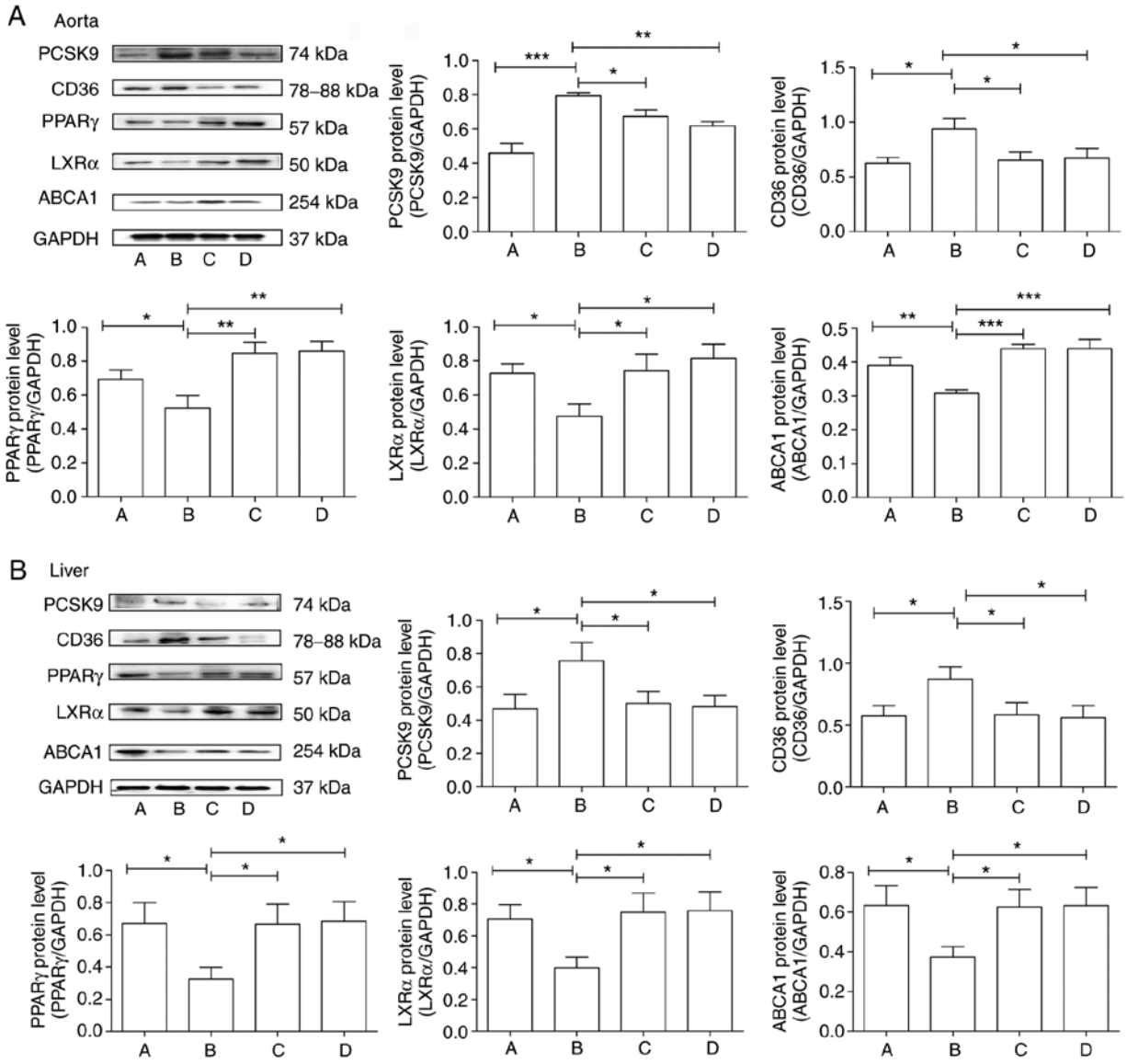

Figure 7. Effect of quercetin on the expression of PCSK9, CD36, PPARγ, LXRα and ABCA1 in mouse (A) aortas and (B) livers. A, Control group; B, model group; C, quercetin group; D, atorvastatin group. Data are presented as the means ± standard deviation, *P<0.05, **P<0.01 and ***P<0.001.

resulted in significant increases in PPARγ, LXRα and ABCA1 protein levels (P<0.05, P<0.01 and P<0.001) and significant decreases in PCSK9 and CD36 protein levels (P<0.05, and P<0.01) as compared with the model group. However, the difference between the quercetin and atorvastatin group was not significant (P>0.05). The results are presented in Fig. 7.

Discussion

Lipid metabolism disorders, particularly RCT-caused disorders, are critical steps in the pathogenesis and development of AS. PCSK9 plays a direct role in ABCA1-mediated RCT and consequently influences relevant steps in atherogenesis (2). CD36 effectively regulates lipid metabolism via promoting HDL synthesis in macrophages, participating in cholesterol efflux and up-regulating ABCA1 expression (10). PPARγ, which is a key regulator of CD36, regulates lipid metabolism via activating LXRα and up-regulating ABCA1 expression (11).

High-fat diet-induced atherosclerosis in apoE$^{-/-}$ mice is one of the most frequently used and well-recognized mouse models of AS. The atherosclerosis developed in this model, including atherosclerotic plaques and lipid deposition, is comparable to the pathogenesis and gradual development of AS in humans (12). As shown in this study, in the apoE$^{-/-}$ mice fed with a high-fat diet, the serum levels of TC, LDL-C and oxLDL increased, while those of HDL-C decreased; H&E staining of the aortic sinus revealed typical atherosclerotic plaques; Oil Red O staining confirmed massive red-stained lipid accumulation in the aortic sinus. Masson's trichrome staining revealed fewer collagen fibers at the aortic root and thinner fibrous caps. Filipin staining indicated increased FC levels in the aortic sinus. In addition, H&E staining of the liver tissue revealed deformed hepatocytes and disorganized cords of hepatocytes; Oil Red O staining revealed massive red-stained lipid droplets; Masson's trichrome staining revealed reduced collagen fibers in liver tissue. The results of western blot analysis demonstrated that the expression levels

of PCSK9 and CD36 were upregulated, while the expression levels of PPARγ, LXRα and ABCA1 were downregulated in both the aorta and liver.

Atherosclerosis is an autoimmune disease with inflammatory responses. TNF-α induces the secretion of inflammatory cytokines, which leads to the thinning of the fibrous cap and thus influences the stability of the plaques (13). IL-6 reduces foam cell formation, enhances the capacity of human macrophages to phagocytose apoptotic cells, and thus influences the pathogenesis and development of AS (14). Studies have shown the potential of IL-10 to arrest and reverse the inflammatory response in established atherosclerosis via inhibiting the production of reactive oxygen intermediates (15). The results of ELISA from this study demonstrated higher serum levels of TNF-α and IL-6 and lower serum levels of IL-10 in the model group mice as compared with the control group mice.

PCSK9 is a member of the proprotein convertase family of proteins that regulates a wide variety of physiopathological processes, which include lipid metabolism, inflammatory responses, glucose metabolism, cell apoptosis and other processes (16). PCSK9 is one of the major targets in the AS research field. A previous study demonstrated that function-acquired transgenic mice have higher serum cholesterol levels and more extensive atherosclerotic plaques compared with PCSK9-deficient transgenic mice (17). PCSK9-deficient C57BL/6 and apoE$^{-/-}$ mice have a lower chance of developing AS compared to PCSK9-overexpressing mice, which have more severe AS presentations (18). CD36 is a scavenger receptor involved in lipid metabolism, immunity, angiogenesis, and other physiopathological processes (19). Since CD36 plays pivotal roles in the initiation and development of atherosclerosis, CD36 serves as an important molecular marker for the diagnosis of AS (20). CD36$^{-/-}$ mice exhibit a significant reduction in the atherosclerotic lesion area throughout the aorta, while the re-introduction of CD36 results in increases in lesion area (21). Elevated levels of PCSK9 stimulate the expression of CD36 and oxLDL uptake in TNF-α treated macrophages, thus contributing to the progression of AS (4). Silencing the expression of PCSK9 using siRNA has been shown to significantly attenuate oxLDL-induced macrophage apoptosis by downregulating the expression of CD36 (22). PPARγ is a ligand-dependent transcription factor which plays an important role in the modulation of lipid metabolism (23). LXRs induce ABCA1 gene expression. They accelerate RCT from tissues to liver and cholesterol excretion as bile acids, and therefore may lead to an atheroprotective effect (24). As a key protein regulating the RCT pathway, ABCA1 modulates lipid metabolism via mediating the reverse transportation of cholesterol to apoAI and promoting HDL formation (25). CD36 mediates the endocytosis of oxLDL, activates the PPARγ-LXRα-ABCA1 pathway, promotes the reverse transportation of excess cholesterol to HDL, accelerates the process of RCT and exerts atheroprotective effects (26). In this study, the results of western blot anlaysis revealed that in the apoE$^{-/-}$ mice fed with a high-fat diet, the PCSK9 and CD36 expression levels increased, while those of PPARγ, LXRα and ABCA1 decreased in both the aorta and liver tissue.

Quercetin is a flavonoid derived from plants including dodder, mulberry and others (27,28). Quercetin has a wide range of biological activities, such as cardiovascular protective effects, anti-atherosclerosis, anti-oxidation, anti-inflammation, increasing coronary blood flow, reducing capillary fragility and other effects (6). A previous study demonstrated that quercetin supplementation significantly reduces cardiac hypertrophy, a cause of cardiovascular morbidity and mortality (29). Recently, the mechanisms of the the anti-atherosclerotic effects of quercetin have been investigated extensively. For example, quercetin has been shown to effectively reduce the serum TC and LDL-C levels elevated by a high-fat diet in a rabbit model and has demonstrated antiatherogenic properties (30). Quercetin significantly reduces the endothelial expression of adhesion molecules induced by oxLDL, attenuated the TLR-NF-κB signaling pathway and thus decreases the inflammatory process in a rabbit model (31). In addition, quercetin has been shown to inhibit atherosclerotic plaque development in high fructose-fed C57BL/6 mice by inhibiting reactive oxygen species (ROS) production and activating the PI3K/AKT signaling pathway (32). Quercetin significantly reduces lipid accumulation and the upregulation of CD36 mRNA and protein expression in oxLDL-activated RAW264.7 macrophage cells (33). Furthermore, quercetin protects macrophage from oxLDL-induced damage by regulating PCSK9 and ABCA1 expression, and thus prevents the progression of AS (7). In addition, quercetin regulates ABCA1 protein expression and increases the HDL-C level via the activation of the PPARγ-LXRα pathway, and consequently reduces the risk of atherogenesis (34,35).

This study demonstrated that in apoE$^{-/-}$ mice fed with a high-fat diet, quercetin treatment significantly reduced the atherosclerotic plaque area, lipid accumulation and FC levels, and increased the collagen fibers in atherosclerotic plaques. In addition, quercetin treatment improved hepatocyte microstructure, reduced the number of lipid droplets, as well as the Oil Red O-stained lipid content in liver tissue, and increased the liver collagen fiber content. Moreover, quercetin treatment resulted in increased serum levels of HDL-C and IL-10, together with decreased serum levels of TC, LDL-C, oxLDL, TNF-α and IL-6. Finally, quercetin treatment resulted in the downregulation of PCSK9 and CD36 protein expression and the upregulation of PPARγ, LXRα and ABCA1 protein expression levels in both the aortic and liver tissue. These results demonstrated that the atheroprotective effects of quercetin may be caused via regulating the expression of PCSK9, CD36, PPARγ, LXRα and ABCA1.

Acknowledgements

Not applicable.

Funding

The present study was supported by grants from the National Natural Science Foundation of China (grant no. 81873348), the Shanghai Nature Science Fund (grant no. 16ZR1433900), the Shanghai Health and Family Planning Commission Fund (grant no. 201640217) and Shanghai University of Traditional Chinese Medicine graduate 'innovation ability training' special research projects (grant no. Y201858).

Availability of data and materials

All data generated or analyzed during this study are included in this published article or are available from the corresponding author on reasonable request.

Authors' contributions

QJ, HC, DS, SL, LY, CC, SX and FD conceived the experiments and experimental plan. QJ, HC, SL and LY performed the experiments and collected and analyzed the data. QJ and HC wrote the manuscript. DS, CC, SX and FD reviewed and edited the manuscript. All authors have read and approved the final manuscript.

Ethics approval and consent to participate

All animal experiments were approved and carried out in strict compliance with the Shanghai University of Traditional Chinese Medicine Institutional Animal Care and Use Committee (IACUC) guidelines (Protocol no. PZSHUTCM18113002).

Patient consent for publication

Not applicable.

Competing interests

The authors declare that they have no competing interests.

References

1. Wang HH, Garruti G, Liu M, Portincasa P and Wang DQ: Cholesterol and lipoprotein metabolism and atherosclerosis: Recent advances in reverse cholesterol transport. Ann Hepatol 16 (Suppl 1: S3-S105): S27-S42, 2017.
2. Adorni MP, Cipollari E, Favari E, Zanotti I, Zimetti F, Corsini A, Ricci C, Bernini F and Ferri N: Inhibitory effect of PCSK9 on Abca1 protein expression and cholesterol efflux in macrophages. Atherosclerosis 256: 1-6, 2017.
3. Chávez-Sánchez L, Garza-Reyes MG, Espinosa-Luna JE, Chávez-Rueda K, Legorreta-Haquet MV and Blanco-Favela F: The role of TLR2, TLR4 and CD36 in macrophage activation and foam cell formation in response to oxLDL in humans. Hum Immunol 75: 322-329, 2014.
4. Ding Z, Liu S, Wang X, Theus S, Deng X, Fan Y, Zhou S and Mehta JL: PCSK9 regulates expression of scavenger receptors and ox-LDL uptake in macrophages. Cardiovasc Res 114: 1145-1153, 2018.
5. He XW, Yu D, Li WL, Zheng Z, Lv CL, Li C, Liu P, Xu CQ, Hu XF and Jin XP: Anti-atherosclerotic potential of baicalin mediated by promoting cholesterol efflux from macrophages via the PPARγ-LXRα-ABCA1/ABCG1 pathway. Biomed Pharmacother 83: 257-264, 2016.
6. Lara-Guzman OJ, Tabares-Guevara JH, Leon-Varela YM, Álvarez RM, Roldan M, Sierra JA, Londoño-Londoño JA and Ramirez-Pineda JR: Proatherogenic macrophage activities are targeted by the flavonoid quercetin. J Pharmacol Exp Ther 343: 296-306, 2012.
7. Li S, Cao H, Shen D, Jia Q, Chen C and Xing S: Quercetin protects against ox-LDL-induced injury via regulation of ABCA1, LXR-α and PCSK9 in RAW264.7 macrophages. Mol Med Rep 18: 799-806, 2018.
8. Lee SM, Moon J, Cho Y, Chung JH and Shin MJ: Quercetin up-regulates expressions of peroxisome proliferator-activated receptor γ, liver X receptorα, and ATP binding cassette transporter A1 genes and increases cholesterol efflux in human macrophage cell line. Nutr Res 33: 136-143, 2013.
9. Tang JM and Chen ML: Medical Laboratory Zoology. China Press of Traditional Chinese Medicine, Beijing, pp276-278, p286, 2012.
10. Yue P, Chen Z, Nassir F, Bernal-Mizrachi C, Finck B, Azhar S and Abumrad NA: Enhanced hepatic apoA-I secretion and peripheral efflux of cholesterol and phospholipid in CD36 null mice. PLoS One 5: e9906, 2010.
11. Majdalawieh A and Ro HS: PPARgamma1 and LXRalpha face a new regulator of macrophage cholesterol homeostasis and inflammatory responsiveness, AEBP1. Nucl Recept Signal 8: e004, 2010.
12. Breslow JL: Mouse models of atherosclerosis. Science 272: 685-688, 1996.
13. Martens FM, Rabelink TJ, op 't Roodt J, de Koning EJ and Visseren FL: TNF-alpha induces endothelial dysfunction in diabetic adults, an effect reversible by the PPAR-gamma agonist pioglitazone. Eur Heart J 27: 1605-1609, 2006.
14. Frisdal E, Lesnik P, Olivier M, Robillard P, Chapman MJ, Huby T, Guerin M and Le GW: Interleukin-6 protects human macrophages from cellular cholesterol accumulation and attenuates the proinflammatory response. J Biol Chem 286: 30926-30936, 2011.
15. Terkeltaub RA: IL-10: An 'immunologic scalpel' for atherosclerosis? Arterioscler Thromb Vasc Biol 19: 2823-2825, 1999.
16. Lan H, Pang L, Smith MM, Levitan D, Ding W, Liu L, Shan LX, Shah VV, Laverty M, Arreaza G, *et al*: Proprotein convertase subtilisin/kexin type 9 (PCSK9) affects gene expression pathways beyond cholesterol metabolism in liver cells. J Cell Physiol 224: 273-281, 2010.
17. Herbert B, Patel D, Waddington SN, Eden ER, McAleenan A, Sun XM and Soutar AK: Increased secretion of lipoproteins in transgenic mice expressing human D374Y PCSK9 under physiological genetic control. Arterioscler Thromb Vasc Biol 30: 1333-1339, 2010.
18. Jänis MT, Tarasov K, Ta HX, Suoniemi M, Ekroos K, Hurme R, Lehtimäki T, Päivä H, Kleber ME, März W, *et al*: Beyond LDL-C lowering: Distinct molecular sphingolipids are good indicators of proprotein convertase subtilisin/kexin type 9 (PCSK9) deficiency. Atherosclerosis 228: 380-385, 2013.
19. Silverstein RL and Febbraio M: CD36, a scavenger receptor involved in immunity, metabolism, angiogenesis, and behavior. Sci Signal 2: re3, 2009.
20. Yazgan B, Ustunsoy S, Karademir B and Kartal ON: CD36 as a biomarker of atherosclerosis. Free Radic Biol Med 75 (Suppl 1): S10, 2014.
21. Febbraio M, Guy E and Silverstein RL: Stem cell transplantation reveals that absence of macrophage CD36 is protective against atherosclerosis. Arterioscler Thromb Vasc Biol 24: 2333-2338, 2004.
22. Tang ZH, Chun-Yan WU, Xie M, Liu LS and Jiang ZS: Effects of PCSK9 siRNA on CD36, SR-A1 and SR-B1 expression in THP-1 derived macrophages. Acta Univ Med Nanjing (Nat Sci) 31: 673-678, 2011.
23. Zhao L, Varghese Z, Moorhead JF, Chen Y and Ruan XZ: CD36 and lipid metabolism in the evolution of atherosclerosis. Br Med Bull 126: 101-112, 2018.
24. Ikhlef S, Berrougui H, Kamtchueng SO and Khalil A: Paraoxonase 1-treated oxLDL promotes cholesterol efflux from macrophages by stimulating the PPARgamma-LXRalpha-ABCA1 pathway. FEBS Lett 590: 1614-1629, 2016.
25. Larrede S, Quinn CM, Jessup W, Frisdal E, Olivier M, Hsieh V, Kim MJ, Van Eck M, Couvert P, Carrie A, *et al*: Stimulation of cholesterol efflux by LXR agonists in cholesterol-loaded human macrophages is ABCA1-dependent but ABCG1-independent. Arterioscler Thromb Vasc Biol 29: 1930-1936, 2009.
26. Zhong Q, Zhao S, Yu B, Wang X, Matyal R, Li Y and Jiang Z: High-density lipoprotein increases the uptake of oxidized low density lipoprotein via PPARγ/CD36 pathway in inflammatory adipocytes. Int J Biol Sci 11: 256-265, 2015.
27. Kong LL, Cui QJ and Yi HX: Measurement of quercetin, kaempferide, and isorhamnetin content in Semen Cuscutae by HPLC. Chin Tradit Herbal Drugs 35: 112-113, 2004 (In Chinese).
28. Lv L, Zhu YM and Xu DM: Study on flavones from Taxillus chinensis (DC.) Danser and assay of its quercetin. Chinese Traditional Patent Medicine 26: 1046-1048, 2004.
29. Han JJ, Hao J, Kim CH, Hong JS, Ahn HY and Lee YS: Quercetin prevents cardiac hypertrophy induced by pressure overload in rats. J Vet Med Sci 71: 737-743, 2009.
30. Juźwiak S, Wójcicki J, Mokrzycki K, Marchlewicz M, Białecka M, Wenda-Rózewicka L, Gawrońska-Szklarz B and Droździk M: Effect of quercetin on experimental hyperlipidemia and atherosclerosis in rabbits. Pharmacol Rep 57: 604-609, 2015.

31. Bhaskar S, Sudhakaran PR and Helen A: Quercetin attenuates atherosclerotic inflammation and adhesion molecule expression by modulating TLR-NF-κB signaling pathway. Cell Immunol 310: 131-140, 2016.
32. Lu XL, Zhao CH, Yao XL and Zhang H: Quercetin attenuates high fructose feeding-induced atherosclerosis by suppressing inflammation and apoptosis via ROS-regulated PI3K/AKT signaling pathway. Biomed Pharmacother 85: 658-671, 2017.
33. Chen M: Effect of quercetin on ox-LDL-induced lipid accumulation and peroxidation in mouse macrophages. Chin J Pathophysiol 29: 1370-1374, 2013 (In Chinese).
34. Sun L, Li E, Wang F, Wang T, Qin Z, Niu S and Qiu C: Quercetin increases macrophage cholesterol efflux to inhibit foam cell formation through activating PPARγ-ABCA1 pathway. Int J Clin Exp Pathol 8: 10854-10860, 2015.
35. Ren K, Jiang T and Zhao GJ: Quercetin induces the selective uptake of HDL-cholesterol via promoting SR-BI expression and the activation of the PPARγ/LXRα pathway. Food Funct 9: 624-635, 2018.